7-2008

Edge effects in four point direct current potential drop measurement

Yi Lu
Iowa State University

John R. Bowler
Iowa State University, jbowler@iastate.edu

Chongxue Zhang
Iowa State University

Nicola Bowler
Iowa State University, nbowler@iastate.edu

EDGE EFFECTS IN FOUR POINT DIRECT CURRENT POTENTIAL DROP MEASUREMENT

Yi Lu, John R. Bowler, Chongxue Zhang, and Nicola Bowler

Citation: AIP Conf. Proc. **1096**, 271 (2009); doi: 10.1063/1.3114215
View online: http://dx.doi.org/10.1063/1.3114215
View Table of Contents: http://proceedings.aip.org/dbt/dbt.jsp?KEY=APCPCS&Volume=1096&Issue=1
Published by the American Institute of Physics.

EDGE EFFECTS IN FOUR POINT DIRECT CURRENT POTENTIAL DROP MEASUREMENT

Yi Lu, John R. Bowler, Chongxue Zhang, and Nicola Bowler

Center for Nondestructive Evaluation, Iowa State University,
Applied Sciences Complex II, 1915 Scholl Road, Ames, IA 50011, USA

ABSTRACT. The four point direct current potential drop (DCPD) technique is used to measure electrical conductivity and crack depth. It is also used, together with Hall voltage measurements, to evaluate carrier concentration and mobility in semiconductors. Here the theory of DCPD is studied for planar structures in which edge effects may have to be taken into account and correction made to ensure accuracy. The current injected at a point on the surface of an infinite plate of finite thickness gives rise to a field that can be expressed as a summation derived using image theory. Because the images are periodic in the direction perpendicular to the plate surface, the field can also be conveniently expressed in the form of a Fourier series. The two basic formulas; image summation and Fourier series, can be modified for the case where the probe points are near the edge of a plate by further applying image theory and summing image/Fourier terms in two dimensions. Both of these approaches agree with measurement results very well.

Keywords: Four-Point Probe, DCPD, Edge Effect, Geometrical Correction Factor, Method of Images, Fourier Series
PACS: 41.20.-q

INTRODUCTION

The direct current potential drop (DCPD) technique is widely used to characterize electrical conductivity of materials in the semiconductor industry [1], in biomedical research [2] and in geophysical applications [3]. Compared with other measurement methods such as eddy-current technology (ECT), DCPD can be applied to measure the conductivity of ferrous metals, being independent of magnetic permeability. Since the measured signal is inversely proportional to the conductivity, a good signal-to-noise ratio can be guaranteed for low-conductivity materials such as semiconductors and geophysical specimens. For DCPD measurements, the four-point probe is one of the most common probe configurations used in practice. Often, although not necessarily, the probe points are arranged in a straight line as shown in Figure 1. Generally, the current is injected and extracted via the outer two pins (P_1 and P_2) and the floating potential drop is measured across the inner two pins (Q_1 and Q_2) with a high input impedance circuit. When the probe is sufficiently far from the boundary of the specimen (eight or nine times the probe length [4]), the current distribution is not significantly disturbed by the boundary. When the probe is close to the boundary, however, the current can be significantly distorted which results in an increase in the measured potential drop. So, even for a uniformly thick specimen, different voltages can be measured at different probe

CP1096, *Review of Quantitative Nondestructive Evaluation Vol. 28,*
edited by D. O. Thompson and D. E. Chimenti

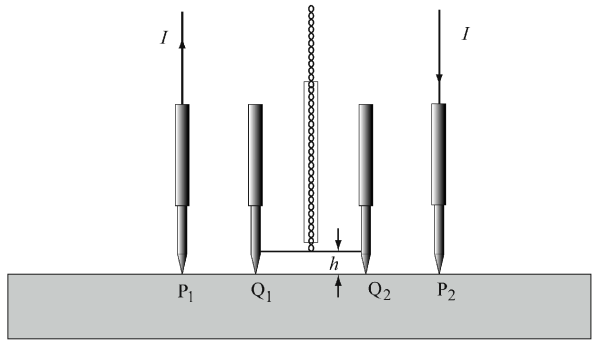

FIGURE 1. Co-linear four-point-probe configuration in DCPD system.

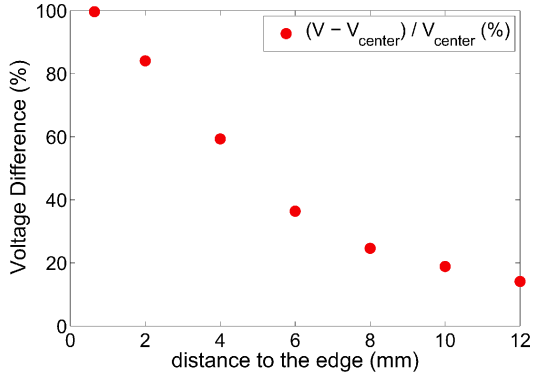

FIGURE 2. Voltage relative difference between experimental results with edge effect and center point in a large thin plate.

positions. Figure 2 shows the relative difference between voltages measured experimentally at the center and near the edge of a large thin plate. The detailed parameters for both the plate and probe utilized in this experiment can be found in Table 1.

For the purpose of modelling the edge effect in four-point DCPD measurements, several approaches have been brought forward. A solution via conformal transformation [5] assumes that the specimen is thin compared to the probe spacing. An analytical solution of the Poisson equation given in reference [6] does not restrict the thickness of the specimen, but the form of the solution is complex and the convergence of the solution is poor for thick samples. A conventional method-of-images solution [7] yields a simple and elegant solution form, but generally converges slowly if at least one dimension of the specimen is small relative to the probe spacing. To improve upon numerical calculation of slowly converging infinite summations, Uhlir [8] evaluated some auxiliary functions and tabulated the potentials of several simple image systems, for ease of reference.

This paper focuses on establishing a theoretical model for the situation in which the probe is close to one edge of a large plate with arbitrary thickness. Previously, an analytical solution for the electric field distribution in a half-space conductor has been formulated in terms of a transverse magnetic (TM) potential [9]. Subsequently, the AC potential drop on the surface of a metal half-space was derived and compared with experimental results [10]. The electric field distribution in a homogeneous conductive plate with uniform thickness was also solved analytically [11] and good agreement with measured AC potential drop was obtained [12]. Here, the method of images is applied to model the edge effect in four-point DCPD

TABLE 1. Probe and plate parameters corresponding to the data shown in Figure 2. L is the separation of the current-carrying electrodes. P is the separation of the voltage pick-up electrodes.

Probe parameters	
L (mm)	18.009 ± 0.003
P (mm)	6.035 ± 0.003
Plate parameters	
Width (mm)	412
Length (mm)	412
Thickness (mm)	1.57 ± 0.01
Conductivity (MS/m)	5.50 ± 0.04

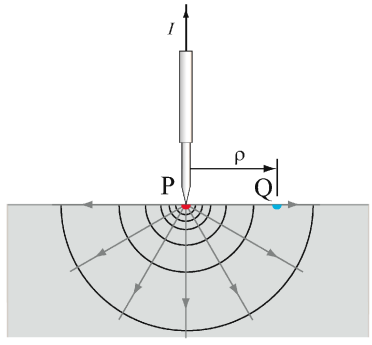

FIGURE 3. Injection of DC current at the surface of a half-space conductor.

and the solution form is simple and elegant. To overcome the mentioned disadvantage of slow convergence, a Fourier Series representation has been employed to obtain much faster convergence for plates thinner than the probe dimension.

THEORY

The theoretical model presented here makes some approximations. First, the connecting wires are represented as filaments. Secondly, current and voltage contacts are modelled as infinitesimal points on the specimen surface, which is flat. Last, the plate is homogeneous, isotropic and has linear material properties. These approximations are shown to be reasonable since the theory agrees well with experimental data as shown later.

Half-space Conductor

First, consider the simple problem shown in Figure 3. Direct current I is injected into a half-space conductor at point P and diverges uniformly. This gives rise to the potential Φ for a point in the conductor given by

$$\Phi = \frac{I}{2\pi\sigma R}, \tag{1}$$

where σ is the conductivity of the conductor and $R = \sqrt{(x-x')^2 + (y-y')^2 + (z-z')^2}$ is the distance from the injection point. Unprimed coordinates represent field points and the source coordinates are primed. Choosing the origin of the coordinate system at the surface of the conductor means that $z = z' = 0$ and $R = \rho = \sqrt{(x-x')^2 + (y-y')^2}$.

In four-point probe problem, the potential at one point is the superposition of potentials due to both injected and extracted currents. So, the potential of a field point Q due to a source

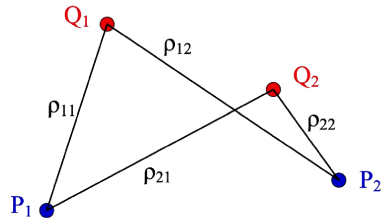

FIGURE 4. Contact points for current (P_i) and voltage (Q_i) electrodes on the surface of a planar specimen (plan view).

of current at P_2 and a sink of current at P_1 on the surface is

$$\Phi(\rho) = \frac{I}{2\pi\sigma} f(\rho), \tag{2}$$

with

$$f(\rho) = \frac{1}{\rho_2} - \frac{1}{\rho_1}, \tag{3}$$

where $\rho_i = \left|\bar{Q} - \bar{P}_i\right| = \sqrt{(x - x_i')^2 + (y - y_i')^2}$ and $i = 1, 2$. In addition, the potential drop V between two points Q_1 and Q_2 on the surface of the specimen due to the current through P_1 and P_2, as shown in Figure 4, can be written with the general form

$$V = \Phi_{Q_2} - \Phi_{Q_1} = \frac{I}{2\pi\sigma} \left[f_2(\rho) - f_1(\rho)\right], \tag{4}$$

where

$$f_i(\rho) = \frac{1}{\rho_{i2}} - \frac{1}{\rho_{i1}}, \tag{5}$$

$\rho_{ij} = \left|\bar{Q}_i - \bar{P}_j\right| = \sqrt{\left(x_i - x_j'\right)^2 + \left(y_i - y_j'\right)^2}$ and $i, j = 1, 2$.

Conductor with Finite Thickness

In the half-space problem, the potential due to a single injected current is given by equation (1), which satisfies the Von Neumann boundary condition $\partial\Phi/\partial z = 0$ on the surface of the conductor, away from the current injection point. For a large plate of thickness $c/2$ whose upper surface is in the plane $z = 0$, Figure 5, there is an additional but similar boundary condition at $z = -c/2$. The method of images is employed to satisfy the conditions on both of these surfaces.

Placing an image source at $z = -c$ of the same polarity as the actual source, yields two opposing currents whose z-components exactly balance in the $z = -c/2$ plane. Thus, with one image source added, the Von Neumann boundary condition at $z = -c/2$ is satisfied. But, the boundary condition at $z = 0$ is no longer satisfied because of the effect of the image source. This effect can be balanced by introducing another image source with the same polarity at $z = c$. In fact it is necessary to add images in this way in both positive and negative z-directions out to infinity. Finally, the images of a current source at P occupy positions with period c in the z-direction as shown in Figure 5.

From the method of images, a source at P_2 and a sink at P_1 give rise to a potential at Q on the surface that is a generalization of equation (3);

$$f(\rho) = \sum_{n=-\infty}^{+\infty} \left[\frac{1}{\sqrt{\rho_2^2 + (nc)^2}} - \frac{1}{\sqrt{\rho_1^2 + (nc)^2}}\right], \tag{6}$$

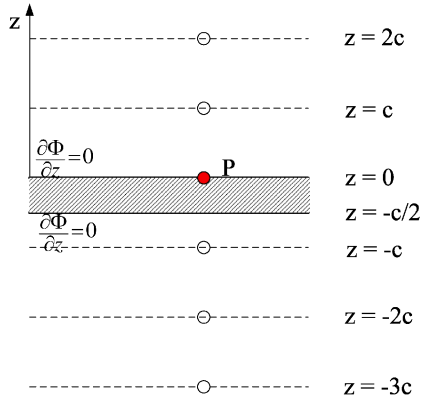

FIGURE 5. Images for an infinite plate with finite thickness c/2.

where $\rho_i = \left|\bar{Q} - \bar{P}_i\right| = \sqrt{(x - x_i')^2 + (y - y_i')^2}$, $i = 1, 2$ and the potential drop can be evaluated as in equation (4). Note, when $c \to \infty$ only the term with $n = 0$ survives in the summations and we obtain

$$f(\rho) = \sum_{n=-\infty}^{+\infty} \left[\frac{1}{\sqrt{\rho_2^2 + (nc)^2}} - \frac{1}{\sqrt{\rho_1^2 + (nc)^2}} \right] \to \left(\frac{1}{\rho_2} - \frac{1}{\rho_1} \right) \tag{7}$$

which agrees with the half-space result (3).

For numerical evaluation, the sum in equation (7) must be approximated by truncating at a finite number of terms. In the case of a thick plate the number of terms needed for good convergence is relatively small, whereas a large number of terms is necessary in the case of a thin plate due to the slow convergence of the summation for thin plates.

Conductor with Finite Thickness and One Edge

When applying the method of images to obtain a solution for the measured potential drop when the probe is near an edge of a conductive plate, it is necessary to satisfy the Von Neumann boundary condition on the three surfaces of the conductor. Let the surfaces be at $(0 \le y \le \infty, z = 0)$, $(0 \le y \le \infty, z = -c/2)$ and $(-c/2 \le z \le 0, y = 0)$, as shown in Figure 6. First, balance the actual source with an image source of the same polarity placed symmetrically on the y-axis. Then, by the argument of the previous section, there are two corresponding groups of images aligned in the z-direction with period c as introduced in Figure 5. Thus the potential at a field point Q due to a current source and sink on the surface $z = 0$ can be written as a generalization of equation (6):

$$f(\rho) = \sum_{j=1}^{2} \sum_{n=-\infty}^{\infty} \left[\frac{1}{\sqrt{\rho_{j2}^2 + (nc)^2}} - \frac{1}{\sqrt{\rho_{j1}^2 + (nc)^2}} \right]. \tag{8}$$

Here, $\rho_{jk} = \sqrt{(x - x_k')^2 + \left[y - (-1)^j y_k'\right]^2}$ with $j, k = 1, 2$. Again, by using equation (4) the potential drop can be obtained. In the limiting case $0 \le y \le +\infty$, $y' \to +\infty$

$$\begin{aligned} f(\rho) \approx \sum_{n=-\infty}^{+\infty} \frac{1}{\sqrt{(x - x_2')^2 + (y - y_2')^2 + (nc)^2}} - \sum_{n=-\infty}^{+\infty} \frac{1}{\sqrt{(x - x_1')^2 + (y - y_1')^2 + (nc)^2}} \\ = \sum_{n=-\infty}^{+\infty} \left[\frac{1}{\sqrt{\rho_2^2 + (nc)^2}} - \frac{1}{\sqrt{\rho_1^2 + (nc)^2}} \right] \end{aligned} \tag{9}$$

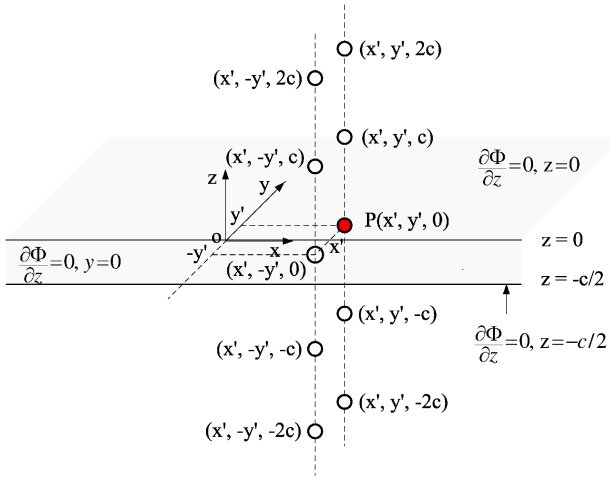

FIGURE 6. Images when close to an edge of a large plate with finite thickness.

where $\rho_i = \left|\bar{Q} - \bar{P}_i\right| = \sqrt{(x - x_i')^2 + (y - y_i')^2}$, $i = 1, 2$, we obtain agreement with the case for a large plate of finite thickness, equation (6).

Fourier Series Representation

The infinite summations (6) and (8) do not converge very quickly for a plate that is thinner than the spacing of the probe points. Convergence can be improved by adopting a Fourier series representation for the infinite sum. The location of the current source and its images shown in Figures 5 and 6 exhibit periodicity in the direction perpendicular to the plate surface, z, with period c. This means that the following identity [13] can be used:

$$\sum_{n=-\infty}^{+\infty} \frac{\exp\left[-\alpha\sqrt{\rho^2 + (z - nc)^2}\right]}{\sqrt{\rho^2 + (z - nc)^2}} = \frac{2}{c} K_0(\alpha\rho) + \frac{4}{c} \sum_{m=1}^{+\infty} K_0\left[\rho\sqrt{\alpha^2 + (2\pi m/c)^2}\right] \cos(2\pi m z/c), \tag{10}$$

in which $K_0(x)$ is the modified Bessel function of the second kind of order zero. Putting $z = 0$ in (10), equation (6) can be transformed to obtain

$$f(\rho) = \frac{2}{c} \ln(\rho_1/\rho_2) + \frac{4}{c} \sum_{m=1}^{+\infty} \{K_0[(\rho_2/c)\, 2\pi m] - K_0[(\rho_1/c)\, 2\pi m]\}. \tag{11}$$

Relation (10) was also used in the theory of four-point alternating current potential drop on a metal plate [14]. Results (6) and (11) provide alternative means of evaluating the potential drop measured between pick-up points of a four-point probe on the surface of a metal plate. The infinite sum in equation (8) can be transformed similarly, to give the following result for a plate with finite thickness and an edge,

$$f(\rho) = \sum_{j=1}^{2} \left\{ \frac{2}{c} \ln(\rho_{j1}/\rho_{j2}) + \frac{4}{c} \sum_{m=1}^{+\infty} [K_0(2\pi m \rho_{j2}/c) - K_0(2\pi m \rho_{j1}/c)] \right\}. \tag{12}$$

Figure 7 compares the convergence of equation (11) with that of equation (6) for a case in which the probe length is 8 times the plate thickness ($L = \rho_1 + \rho_2 = 8c$). In general, equation (11) is much more efficient for computing the potential in the case of a plate with thickness smaller than the probe point separation.

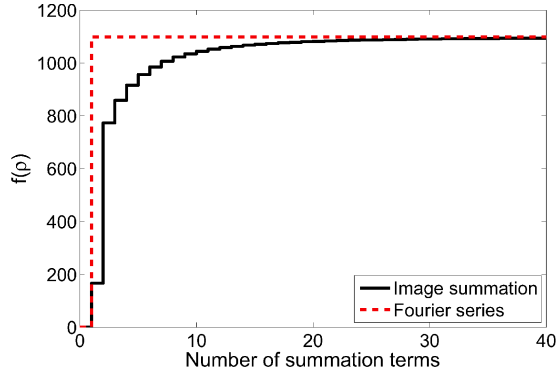

FIGURE 7. Image summation (6) converges slowly compared with Fourier series representation (11) in this case where $\rho_1 = 6c$, $\rho_2 = 2c$, $c = 2mm$.

Limiting Case of a Thin Plate

It is possible to show that only the first term on the right-hand side of equation (11) is significant when the plate thickness $c/2$ is significantly smaller than the separation between the probe points ρ_i. For large argument x, the following asymptotic expansion for $K_0(x)$ [15] holds:

$$K_0(x) \sim \sqrt{\frac{\pi}{2x}} e^{-x} \left(1 - \frac{1}{8x} + \ldots\right), \qquad x \gg 0. \tag{13}$$

The exponential factor including the dimensionless parameter ρ/c is sufficient to make the summation significantly smaller than the first term in equation (12) when $\rho/c \gg 1$ and

$$f(\rho) \approx \frac{2}{c} \ln(\rho_1/\rho_2), \qquad \rho/c \gg 1. \tag{14}$$

This result agrees with that shown in reference [16], which followed the work of Uhlir [8].

EXPERIMENT

A co-linear symmetric four-point-probe measurement system was designed to verify the theory, as shown in the schematic diagram Figure 1. Four sprung, point contacts were mounted in a plastic support block, perpendicular to the surface of a large spring-steel plate. The pin separations were measured with a travelling microscope. Parameters of the plate and probe are listed in Table 1.

In the experiment, a low-frequency alternating current was used rather than direct current, due to several experimental advantages. Full experimental details are given in reference [12], where it is shown that the DC theory is valid for AC when the frequency is below a certain value that depends on the experimental parameters.

In order to validate the theory, both the current through the probe and voltage drop between the pick-up probes must be measured. The first can be can be monitored by measuring the voltage drop across a precision resistor in series with the drive circuit. The latter can be measured by a high input impedance circuit. Values of DCPD both in the center and close to one edge of the plate were measured, with the probe oriented parallel to the edge. The experimental data are compared with theory in Figure 8. In the figure, an obvious edge effect is observed and good agreement between theory and experimental data shows that the edge effect is accurately predicted by the theory.

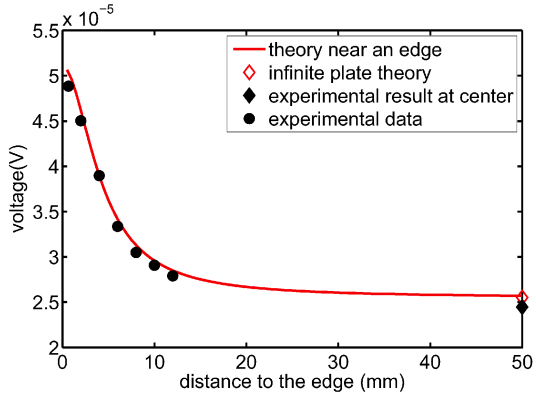

FIGURE 8. Comparison between theory and experimental data. Edge effect theory is got from equation (14) and the infinite plate theory from equation (11).

CONCLUSION

In this paper, an analytical solution has been presented to model edge effects in DCPD measurements on metal plates with finite thickness. A method-of-images solution converges quickly for plates somewhat thicker than the probe dimensions. A Fourier series summation converges more quickly for thinner plates. In future work, DCPD for finite rectangular blocks and layered cylindrical samples will be studied.

ACKNOWLEDGMENT

This work was supported by the NSF Industry/University Cooperative Research program at Iowa State University's Center for Nondestructive Evaluation.

REFERENCES

1. D. K. Schroder, *Semiconductor Material and Device Characterization* (1998).
2. Y. Wang, P. Schimpf, D. Haynor, and Y. Kim, *IEEE Trans. BioMed Eng.* **45**, 877–884 (1998).
3. D. S. Parasnis, *Principles of Applied Geophysics 5th edn* (1997).
4. N. Bowler and Y. Huang, *Four-point alternating current potential drop measurements on metal plates: experiment and interpretation*, Center for Nondestructive Evaluation, Iowa State University, Ames, Iowa 2005. Unpublished.
5. D. S. Perloff, *Solid State Electron.* **20**, 681–687 (1977).
6. M. Yamashita and M. Agu, *Jpn. J. Appl. Phys.* **23**, 1499–1504 (1984).
7. L. B. Valdes, *Proc. of the IRE* **42**, 420–427 (1954).
8. A. Uhlir, *Bell Syst. Tech. J,* (1955).
9. N. Bowler, *J. Appl. Phys.* **95**, 344–348 (2004).
10. N. Bowler, *J. Phys. D Appl. Phys.* **39**, 584–589 (2006).
11. N. Bowler, *J. Appl. Phys.* **96**, 4607–4613 (2004).
12. N. Bowler and Y. Huang, *IEEE Trans. Mag.* **41**, 2102–2110 (2005).
13. R. Sperb, *An Alternative to Ewald Sums. Part I: Identities for Sums.* (1996).
14. J. R. Bowler and N. Bowler, *Proc. R. Soc. A* **463**, 817–836 (2007).
15. A. Jeffery and H. Dai, *Handbook of Mathematical Formulas and Integrals.* (2008).
16. N. Bowler, *Res. Nondestr. Eval.* **17**, 29–48 (2006).